SnT 2019
CTBT: SCIENCE AND TECHNOLOGY CONFERENCE

Upper mantle imaging with surface wave diffraction: AlpArray seismic network and the Cameroon Volcanic Line

Petr Kolínský[1], Felix M. Schneider[2], Götz Bokelmann[1] and the AlpArray Working Group[3]

[1]Department of Meteorology and Geophysics, University of Vienna, Austria,
[2]Department of Geophysics, Helmholtz Centre Potsdam, GFZ, Germany
[3]www.alparray.ethz.ch

petr.kolinsky@univie.ac.at

T1.2-P120

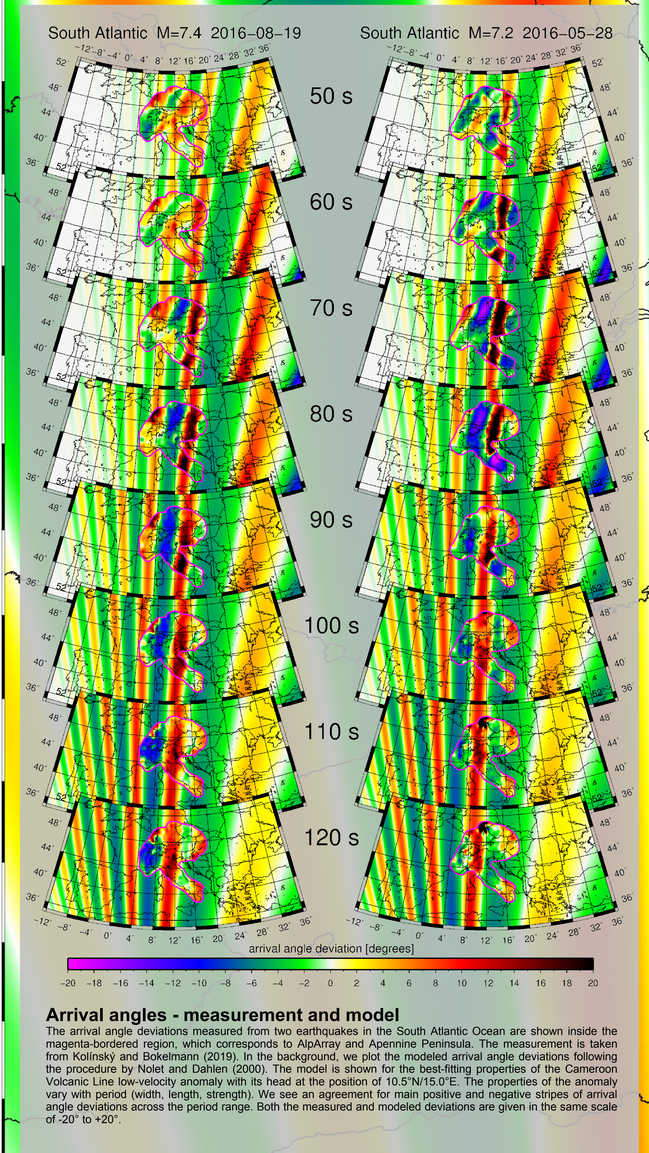
Summary

The AlpArray seismic network stretches hundreds of kilometers in width and more than thousand kilometers in length. It is distributed over the greater Alpine region (Europe) and consists of around 250 temporary and around 400 permanent broadband stations with interstation distances around 40 km. The density of the network allows to track the distortion of travel times and azimuthal deviations of long-period surface waves (30 – 150 s).

We utilize an array beamforming technique for surface waves. The signal is well-recognized and the fundamental mode for Rayleigh waves is separated before the beamforming. We identify the frequency-dependence of surface wave phase velocity and the true directions of propagation. We consider each AlpArray station as a centre of a subarray of neighboring (~ 13) stations with a diameter of 80 km. This allows us to calculate the local phase velocity for more than 500 stations included in the AlpArray project. As we have the full vector of phase velocity (true direction as well as the absolute value of the velocity), we can observe deviations of the backazimuths with respect to the great circles for each subarray. These deviations are frequency-dependent throughout the whole region and form intriguing stripe-like patterns.

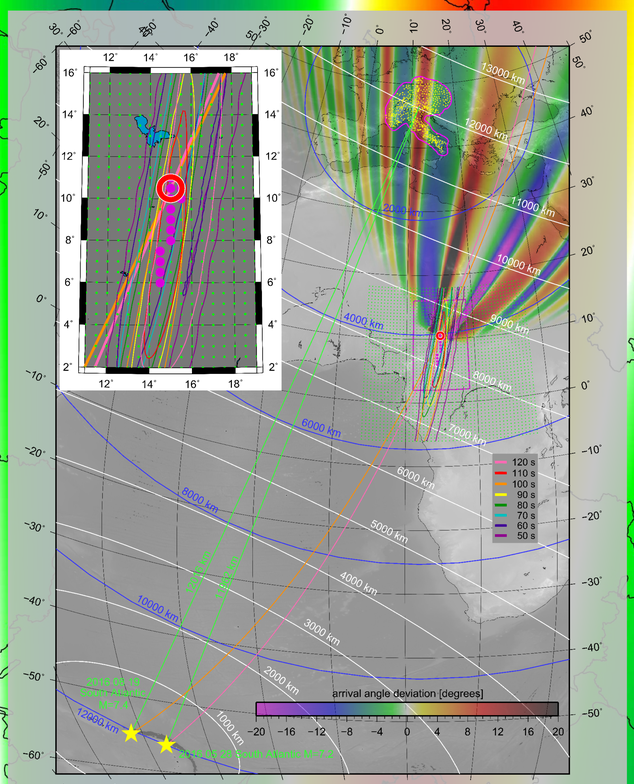
We test a hypothesis that these stripe-like arrival-angle deviation patterns are caused by interference of diffracted wavefield after passing a single small-scaled velocity anomaly. We use Rayleigh waves from two earthquakes under the Southern Atlantic Ocean. Around 500 subarrays of 160 km aperture covering the broader Alpine region are used for beamforming at 15 discrete periods between 50 and 120 s. A grid search inversion scheme is set up for determining characteristics of the anomaly, which is found to be at 10.5°N/15.0°E. Trade-offs between the location, width and phase-time delay of the anomaly are discussed. The width of the anomaly is between 320 – 420 km. For a velocity perturbation associated with the anomaly, we determined its length, which matches the 2500 km long upper mantle low-velocity region under the volcano-capped swells of the Cameroon Volcanic Line.

The observation serves not only as a detector of upper mantle heterogeneities, but it also allows to determine how phase and group travel time delays and wavefront healing can affect global and regional tomographic studies. It has important consequences for the local phase-velocity measurements as well.



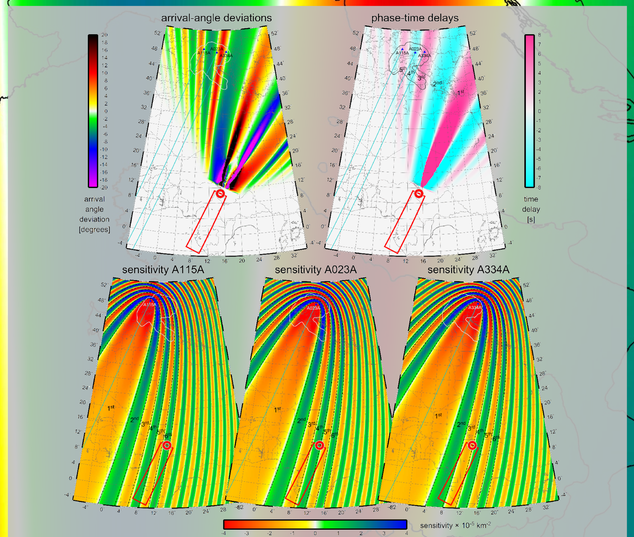
Arrival angles - measurement and model

The arrival angle deviations measured from two earthquakes in the South Atlantic Ocean are shown inside the magenta-bordered region, which corresponds to AlpArray and Apennine Peninsula. The measurement is taken from Kolínský and Bokelmann (2019). In the background, we plot the modeled arrival angle deviations following the procedure by Nolet and Dahlen (2000). The model is shown for the best-fitting properties of the Cameroon Volcanic Line low-velocity anomaly with its head at the position of 10.5°N/15.0°E. The properties of the anomaly vary with period (width, length, strength). We see an agreement for main positive and negative stripes of arrival angle deviations across the period range. Both the measured and modeled deviations are given in the same scale of -20° to +20°.



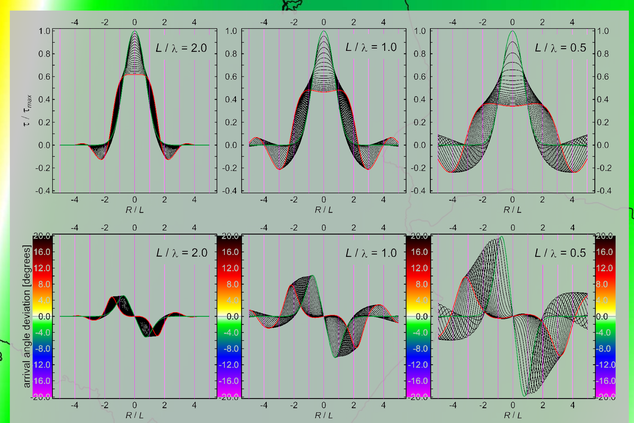
Diffraction on a global scale

Diffraction arrival-angle deviation pattern, the two earthquakes in this study, the AlpArray network in Europe, great circle raypaths (green), distances from the source (white) and from AlpArray (blue). Also shown is the inversion grid, as well as confidence intervals for different periods (detail in the inset).



Equivalence to sensitivity kernels

Arrival-angle deviations (top-left) and time delays (top-right) for a 80 s surface wave traversing the low-velocity anomaly as obtained by the inversion (red box). The bottom maps show sensitivity kernels for three AlpArray stations. Fresnel zones are shown by dashed lines. We see that the sensitivity kernels for these three stations are hitting the CVL anomaly by alternating branches of positive and negative stripes exactly in the manner as the CVL is casting the positive and negative stripes over the AlpArray. For station A334A, the CVL anomaly lies in the 3rd Fresnel zone (orange) slowing down the wave, which corresponds to the fact, that A334A lies at the maximum of the phase-time delays (dark pink stripe in the upper map). Sensitivity for A023A is dominated by the "fast" (green) 4th Fresnel zone of the sensitivity, although both "slow" 3rd and 5th zones contribute a bit as well. For A115A, the CVL anomaly reaches already up to 6th Fresnel zone, however, the "slow" 5th one contributes the most.



Delay times and arrival angles

Evolution of phase-time delay with propagation distance for the three values of width-to-wavelength ratio L/λ. The horizontal axis is the scaled cross-path distance R/L. 20 curves give the effect at scaled propagation distances ranging from x/L = 0 (green curve) to x/L = 9.5 (red curve). Bottom plots: corresponding arrival-angle deviations.

Modeling

The anomaly is a simple box-car heterogeneity placed in a homogeneous space (2D model). The velocity of the surrounding medium as well as the properties of the anomaly vary with period T and hence with depth representing a 3D structure. Properties of the perturbed wavefield at a selected period are controlled by three parameters, the half width of the anomaly $L(T)$, the initial time delay $\tau_{max}(T)$ of the wave right after passing the anomaly and the phase velocity $c(T)$ around the anomaly.

Q as a function of distance x along the ray, distance R perpendicular to the ray, and angular frequency ω, is given as a perturbation to a unit plane wave travelling with a phase velocity c (fixed to the PREM in our computation). It has the form:

$$1 + Q(x, R, \omega) = 1 + \frac{e^{i\omega\tau_{max}} - 1}{\sqrt{\frac{i\lambda x}{\pi L^2} + 1}} \cdot \exp\left[-\frac{\left(R/L\right)^2}{1 + \frac{i\lambda x}{\pi L^2}}\right]$$

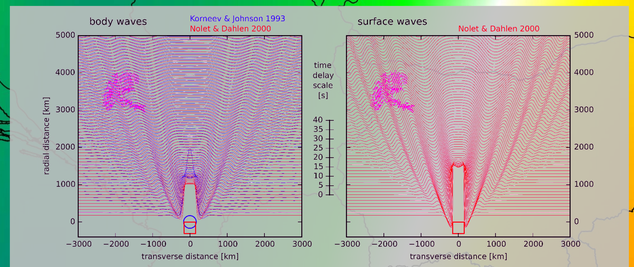
The phase delay $\omega\tau$ of the perturbed wave with respect to the original wave is then given as the phase of the complex perturbed wave

$$\omega\tau(x, R, \omega) = \arctan\left[\frac{\mathrm{Im}(1+Q)}{\mathrm{Re}(1+Q)}\right]$$

We can predict the arrival-angle deviation A at any location x and R for any period T (frequency ω) as

$$A(x, R, \omega) = \arctan\left[\frac{\mathrm{d}w}{\mathrm{d}R}\right] = \arctan\left[c\frac{\mathrm{d}\tau}{\mathrm{d}R}\right]$$

where $w(x,R,\omega) = c\tau(x,R,\omega)$ is the wavefront position. As the velocity c is constant in our computation, the lateral derivative of the wavefront position w can be replaced by the lateral derivative of the phase delay time τ. In our model, x is the distance of the point of interest from the anomaly measured along the great circle from the epicenter (white circles around the M7.4 earthquake for every 1000 km in the figure on the left). R is the lateral distance from the ray which directly hits the anomaly (measured along these white circles).



Comparison of two modeling methods

Left panel: comparison of the exact analytic solution by Korneev and Johnson (1993), (blue) and by the technique by Nolet and Dahlen (2000), (red) for body waves. Right panel: Nolet and Dahlen (2000) technique for surface waves. AlpArray stations are shown as magenta triangles in a position corresponding to the CVL-AlpArray geometry. We see an overall good agreement of the two techniques. They start to differ for larger lateral distances, and there is a difference right at the central region behind the anomaly itself.

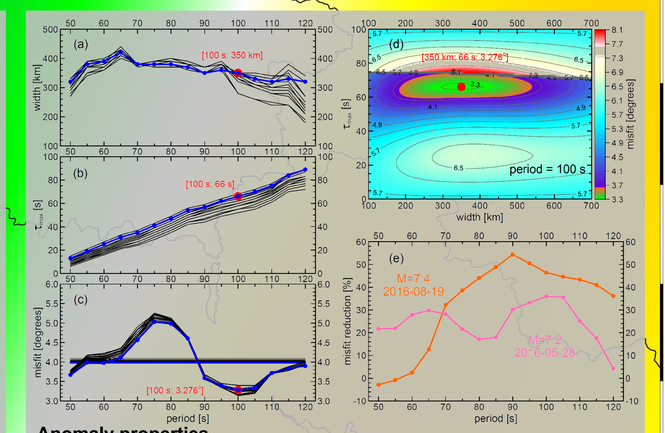
Inversion

We use a grid search for the inversion. Using Rayleigh waves measured on the vertical component, we considered v_{SV} from anisotropic PREM (omitting the water layer), and fixed $c(T)$ to that model for all investigated periods.

We designed a grid of locations covering a large area around the distance of 4000 km where the anomaly was expected to be, see green dots in the figure on the left. The grid consists of points placed 0.5° apart between 4°E – 28°E and 6°S – 18°N, which is 49 x 49 = 2401 locations in total. For each of the locations, we browsed through all combinations of L and τ_{max}. The ranges were 100 – 460 km with a step of 20 km for the width and 6 – 100 s with a step of 2 s for τ_{max} resulting in more than 2 million cases. For each case, we predicted the angular deviations for all our stations (around 500) and for both earthquakes. We computed the misfit (L1 norm) between the observed and predicted deviations and we searched for the best-fitting combination of parameters. Inversion was carried out for each period separately.

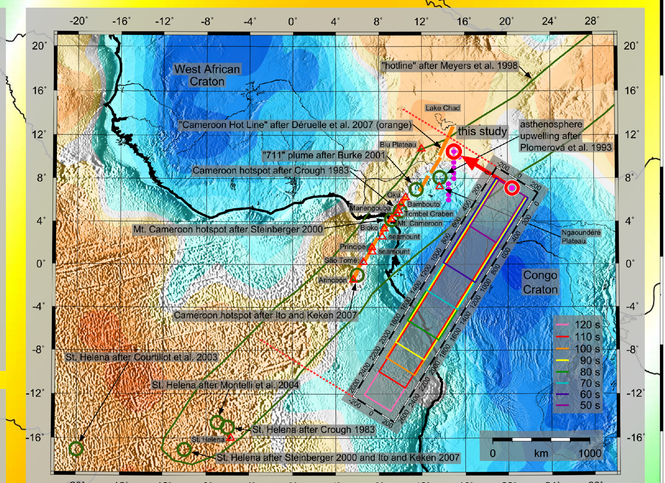
To reach a final location common to all periods, we defined the confidence regions where the misfit differs by less than 10% from the misfit of the best location for the given period. The procedure was repeated with a step of 5 s in period for fifteen values from 50 to 120 s. The confidence regions are plotted in the figure on the left by rainbow colors for only eight periods with a step of 10 s to keep the figure legible. Inset shows the detail of the region where all the suitable areas overlap. Magenta dots represent 13 points on the grid, which lie in the spatial intersection of all 15 confidence regions.

The red circle represents the point with the smallest average misfit over all periods. This point, located at 10.5°N and 15.0°E is considered as the location of the anomaly (anomaly head). The transparent color map then shows the predicted arrival-angle deviations for a 100 s wave for the M7.4 event as an example showing the pattern in a global scale. Orange great circle is an axis of symmetry of that pattern. The period-dependent arrival-angle deviations predicted for the best-fitting widths and time delays found for the final location are shown behind the observed arrival-angle deviations in the leftmost figure.



Anomaly properties

The resulting model: widths (a), time delays (b), and misfits (c) for the 13 locations shown in the left (global) figure. Blue lines represent results for the best-fitting location (shown by a red circle). (d) shows misfit for the width-τ_{max} plane in model space. (e) shows misfit reduction as a function of period, for each earthquake separately.



Cameroon Volcanic Line

Modeled position of the anomaly head (red circle at the location of minimum mean misfit), on a geographic map with topography showing the Cameroon Volcanic Line (triangles represent volcanoes). Also shown is a tomographic model from Debayle et al. (2016). The inset shows the resulting lengths and widths, for each period (colored rectangles). Position of hotspots, plumes and hotlines (both Cameroon hotspot as well as St. Helena hotspot) after different studies are also presented. As the period is longer reaching deeper in the upper mantle, the observed anomaly is longer and narrower.

Conclusion

Using surface-wave data from the AlpArray in Europe, we have identified a low-velocity anomaly, which is associated with the Cameroon Volcanic Line, at large distance from the AlpArray. The main goal of our study had been to test the hypothesis that stripe-like arrival-angle deviations that are generally observed in dense-array data can be attributed to wave interference caused by single distant anomaly. This hypothesis is strongly confirmed. At the same time, we obtain important information on that interesting tectonic feature, which is visible for waves between 50 and 150s. The low-velocity anomaly under the CVL has a length between 570 and 2600 km, getting longer with depth, while its width is around 370 km, narrowing for larger depths. This image of the CVL is generally similar to more recent tomographic models of the region, yet it provides additional insights due to the sharpness of the new constraints.

References

• Kolínský, P., G. Bokelmann and the AlpArray Working Group (2019), Arrival angles of teleseismic fundamental mode Rayleigh waves across the AlpArray, *Geophys. J. Int.*, 218, 114-144, doi: 10.1093/gji/ggz081.

• Nolet, G. and F. A. Dahlen (2000), Wave front healing and the evolution of seismic delay times, *J. Geophys. Res.*, Vol. 105, No. B8, 19,043-19,054, doi:10.1029/2000JB900161.

• Korneev, V. A. and L. R. Johnson (1993), Scattering of elastic waves by a spherical inclusion-I. Theory and numerical results, *Geophys. J. Int.*,115, 230-250, doi:10.1111/j.1365-246X.1993.tb05601.x.

Disclaimer

The views expressed on this poster are those of the author and do not necessarily reflect the view of the CTBTO

PUTTING AN END TO NUCLEAR EXPLOSIONS